Locomotor resilience through load-dependent modulation of muscle co-contraction

Yannick Günzel[1,*], Josef Schmitz[1,2], Volker Dürr[1,2,‡]

[1]Department of Biological Cybernetics, Faculty of Biology, Bielefeld University, Bielefeld 33615, Germany

[2]Cognitive Interaction Technology Center of Excellence, Bielefeld University, Bielefeld 33615, Germany

[*]Present address: Department of Biology, University of Konstanz, 78457 Konstanz, Germany

[‡]Corresponding author: Volker Dürr

Department of Biological Cybernetics, Faculty of Biology, Bielefeld University, Bielefeld 33615, Germany

Email: volker.duerr@uni-bielefeld.de

We show that stick insects compensate for different types of transient changes in load distribution by graded adjustment of muscle co-contraction rather than by a sudden switch in coordinated motor activity.

ABSTRACT

Terrestrial locomotor behavior in variable environments requires resilience to sudden changes in substrate properties. For example, walking animals can adjust to substantial changes in slope and corresponding changes in load distribution among legs. In insects, slope-dependent adjustments have mainly been examined under steady-state conditions, whereas the transition dynamics have been largely neglected. In a previous study, we showed that steady-state adjustments of stick insects to ±45° slopes involve substantial changes in joint torques and muscle activity with only minor changes in leg kinematics. Here, we take a close look at the time course of these adjustments as stick insects compensate for various kinds of disturbances to load distribution. In particular, we test whether the transition from one steady state to another involves distinct transition steps or follows a graded process. To resolve this, we combined simultaneous recordings of whole-body kinematics and hind leg muscle activity to elucidate how freely walking *Carausius morosus* negotiated a step-change

in substrate slope. Step-by-step adjustments reveal that muscle activity changed in a graded manner as a function of body pitch relative to gravity. We further show analogous transient adjustment of muscle activity in response to destabilizing lift-off events of neighboring legs and the disappearance of antagonist co-activation during crawling episodes. Given these three examples of load-dependent regulation of antagonist muscle co-contraction, we conclude that stick insects respond to both transient and sustained changes in load distribution by regulating joint stiffness rather than through distinct transition steps.

INTRODUCTION

Navigating complex environments requires flexible control of the interaction between limbs and substrate. A key aspect of this interaction is the load distribution among the legs with ground contact. It requires sustained, steady-state adjustment to a given substrate, *e.g.*, as load distribution changes with substrate slope (insects: Full and Tullis, 1990; Seidl and Wehner, 2008; Weihmann and Blickhan, 2009; Mendes et al., 2014; Dallmann et al., 2019; mammals: Gregor et al. 2006; Lay et al. 2007), but also transient adjustments on a step-by-step basis, as each foot lift-off causes load transfer among legs (Zill et al., 2009; Dallmann et al., 2017) and may affect stability (Szczecinski et al., 2018). Here, we test whether the same mechanism may explain resilience to both sustained and transient changes in load distribution. If so, we expect to find the same change in muscle activity during the transition from one steady state to another and in response to transient disturbances.

Theoretical and engineering studies suggest that load transfer among neighboring legs is sufficient to entrain coordinated stepping even without neural coupling (Ekeberg and Pearson, 2005; Owaki et al., 2013, 2017). Further, experimental studies show that touch-down events induce load transfer between ipsilateral leg pairs (Zill et al., 2009) in a manner that can support temporal coordination in walking (Dallmann et al., 2017). There is strong evidence that walking insects continuously monitor the load on each leg by strain-sensitive campaniform sensilla (CS; Ridgel et al., 1999, 2000; Zill et al., 2004) and that CS afferent activity changes with substrate slope (Noah et al., 2001). Thus, it could be possible that neuromuscular activity downstream of CS afferents responds similarly to transient load transfer among legs and sustained changes in load distribution as a function of body pitch relative to gravity.

In a previous study, we showed that stick insects experience substantial changes in joint torques when walking on upward or downward slopes, with little or no difference in walking speed and body posture (Dallmann et al., 2019). Since the observed change in joint torques correlated with a sustained change in the activity ratio of two antagonistic muscles, we concluded that persistent changes in load distribution were compensated by regulation of antagonist muscle co-activity. This was supported by preliminary single-trial results that suggested a gradual change of antagonist co-

activity rather than interspersed distinct transition strides. The latter have been proposed for some mammals prior to stepping onto a slope (Gottschall and Nichols 2011). Accordingly, our first objective was to build on our preliminary data and to identify parameters that vary as a continuous function of body pitch when insects transition between two steady states. Second, we relate the principle underlying slope-dependent changes in motor activity to transient changes due to load transfer during horizontal walking and to other gait-related changes in motor activity.

We do so by combining recordings of antagonistic hind leg muscle activity with 3D motion capture of freely walking *Carausius morosus* in response to a step-change in walkway slope by ±45°, both upward and downward. Owing to their size, stick insects permit a detailed analysis of whole-body kinematics (Theunissen and Dürr 2013) and muscle activity (Dallmann et al. 2017) during unrestrained locomotion. Muscle activity was recorded from the antagonistic muscle pair that governs forward/backward movement of the leg: *retractor* and *protractor coxae*. We focused on hind legs, as they attach closely to the center of mass and are important for propulsion and posture control (Cruse, 1976; Dallmann et al., 2016). Apart from monitoring muscle activity time courses, we applied an activation dynamics model for insect muscle (Harischandra et al., 2019) to estimate the time course of co-activation of the antagonist muscle pair during free walking. Assuming that hind leg kinematics change very little as stick insects walk on different slopes (Dallmann et al., 2019), we reasoned that any slope-dependent change in muscle co-activation should reflect a slope-dependent change in co-contraction. With this rationale, we used muscle co-activation as a proxy for thorax-coxa joint stiffness, i.e., the ability of the joint to resist passive deflection.

We show that muscle activity changes continuously with increasing/decreasing body pitch, with a graded decrease in co-contraction throughout the traversal. Since the exact same change in co-contraction occurs during transient responses to load transfer due to lift-off events or during crawling, we conclude that resilience to both transient and sustained changes in load distribution is achieved by the same mechanism of load-dependent regulation of joint stiffness.

METHODS

To evaluate the load-dependent adjustments of freely walking female stick insects (*Carausius morosus*, de Sinéty 1901; Fig. 1) in response to a step-change in slope (either 45° upwards or -45° downwards), recordings of muscle activity were combined with 3D motion capture. During the transition from level to slope walking, the effects on kinematic parameters and muscle activity of the right hind leg were examined on a step-by-step basis. Nine adult, female stick insects (body mass: 0.93 ± 0.19 g.; hind leg femur length: 14.30 ± 0.51 mm; mean ± s.d.) were tested. Animals were reared under constant conditions in a laboratory colony with a 12:12 h light/dark cycle. Experiments

were conducted under constant conditions with an average temperature of 26.9 ± 1.4 °C (mean ± s.d.) and average humidity of 37 ± 3 % (mean ± s.d.).

Manual annotation of trials and specification of step categories

Unrestrained animals walked along a wooden walkway that allowed the transition from steady-state level walking to steady-state walking on a slope (Fig. 1). By careful examination of complementary digital videos, lift-off and touch-down timings for all six legs were annotated manually. Based on the movements of individual legs, steps of the right hind leg were categorized as either steady-state steps or transition steps: Steady-state steps were defined as hind leg step cycles during which all legs were stepping on the same part of the setup, either the horizontal part or the slope. All other steps were defined as transition steps and further categorized based on which leg of the right side was next to swing toward the inclined part of the setup. Hind leg step cycles during which only the ipsilateral front leg swung toward the inclined part were defined as "first transition" steps. Accordingly, hind leg step cycles during which the ipsilateral middle leg swung toward the incline were defined as "second transition" steps. Finally, hind leg step cycles during which the hind leg itself swung to the incline were defined as "third transition" steps. This resulted in five possible step categories for both slope conditions: steady-state level walking, steady-state slope walking, and three transitions steps separating the two steady states. Step cycles during which searching movements of one of the six legs or ground contact of the thorax occurred were excluded from the analysis (except for Fig. 7). Moreover, only those trials that comprised at least one valid step during steady-state level walking and at least one step of another category were considered. According to these criteria, muscle activities (see below) of each category could be related directly to level walking on a trial-by-trial basis, thus accounting for possible differences between recordings.

Recording and post-processing of kinematic data

Movements of the whole body were recorded by tracking the 3D positions of 18 light-weight, retro-reflective markers (mass: 4 mg; diameter: 1.5 mm) with a commercial high-speed motion capture system comprising eight cameras, sampling at 200 fps (Vicon MX10 with T10 cameras; Nexus 1.8.5; Vicon, Oxford, UK). Spatial accuracy of 3D marker localization was approximately 0.1 mm. Markers were attached to the body and leg segments of the animal (Fig. 1, A): Three markers were attached to the metathorax (T3), one to the mesothorax (T2), prothorax (T1), head (Hd), each femur, and each tibia. Marker coordinates were post-processed in MATLAB (version 2018a, TheMathWorks, Natick, MA, USA). Leg kinematics were calculated by adopting a 3D rigid link model (Dallmann et al., 2016). Additionally, a digital video camera (A602fc, Basler, Ahrensburg, Germany) was used to record a

complementary, synchronized side-view video at 100 fps for visual validation and movement annotation.

Hind leg joint angle time courses were divided into swing and stance movements based on careful manual annotation of all trials. The resulting intervals were resampled to the average duration (swing: 160 ms; stance: 730 ms; sampling rate: 200 Hz) of the respective movement, using shape-preserving, piecewise cubic interpolation.

Recording and post-processing of muscle activity

Simultaneously with whole-body kinematics, electromyograms (EMGs) of the retractor and protractor muscles of the right hind leg were recorded. For each muscle, a pair of steel electrodes (50 µm diameter, insulated except for the tip) was implanted through small holes in the metathoracic cuticle (Fig. 1, B). Correct electrode placement was verified by testing resistance reflex responses to imposed movements of the thorax-coxa (ThC) joint. Dental glue (Protemp II, 3M ESPE, St. Paul/MN, USA) held the electrodes in place. To ensure unrestrained walking, a light-weight EMG backpack (aluminum hook; weight: approx. 50 mg; see Dallmann et al., 2017) was used to direct the wires to the amplifiers (Fig. 1, A & B). The backpack was positioned close to the mean center of mass (CoM) of the walking animal, just behind the hind leg coxae, and fixated with beeswax. A custom-built amplifier (MA102, Electronics Workshop, Zoological Institute, Cologne, Germany) was used to amplify (3000-fold) and filter EMG signals (50 Hz notch, 250 Hz high-pass, 7.5 kHz low-pass) which, subsequently, were A/D converted (Power 1401 mk II; Cambridge Electronic Design, Cambridge, UK) and recorded with Vicon Nexus (Version 1.8.5, Vicon, Oxford, UK) at a sampling rate of 6 kHz.

For the later analysis, raw EMG signals were first corrected for a possible baseline shift. Subsequently, signals were rectified and then smoothed with a temporal first-order low-pass filter (τ = 25 ms). Next, the recordings were divided into swing and stance movements and resampled to the respective average duration as described for joint angle time courses above. Finally, rectified and smoothed signals of steps in each category were normalized to level walking. For this, signals were set in relation to the average magnitude from the corresponding step(s) during level walking of the respective trial.

Estimation of muscle activation and joint stiffness

To estimate muscle co-contraction and its load-dependent modulation during walking on inclines, we applied a computational model of muscle activation dynamics. Since steady-state limb kinematics was found to differ only little between level walking and walking on inclines of ±45° (Dallmann et al., 2019), we neglected length dependence of muscle activation and contraction dynamics and opted for the Hatze-Zakotnik model (Zakotnik et al., 2006) that takes account of non-linear force potentiation

for low to medium spike frequencies (Harischandra et al., 2019). To this end, we applied the IMADSim toolbox for MATLAB (Harischandra, 2019) with the parameter set of Zakotnik et al., (2006) to transform spike trains from measured EMG traces into a continuous function of muscle activation over time, for both the retractor and protractor muscle. The binary input signal was generated by detecting peaks in raw EMGs according to an amplitude threshold and representing each of these events by a unit pulse of 1 ms width. The modeled time courses of muscle activation were processed in the same manner as the filtered EMG data, *i.e.*, by resampling to standardized swing and stance duration and subsequent normalization to the average magnitude during level walking (see above).

The term joint stiffness will be used qualitatively as the ability to counteract passive deflection. Owing to the non-linear force-length curves of muscle, and the fact that muscle activation increases the slope of the force-length curve, co-activation of antagonist muscles leads to an increase in joint stiffness without affecting the equilibrium position of the joint (Bührmann and Di Paolo, 2006). Accordingly, we use the estimate of antagonist co-activation as a proxy for joint stiffness.

Statistical analysis

All analyses were calculated in MATLAB. If not stated otherwise, averages represent grand means (means of animal means) with error bars and shaded areas indicating bootstrapped 95 % confidence intervals with $B = 5'000$ samples. Violin plots show probability density estimates based on the bootstrap samples. The range of the violins was bounded to the observed minimum and maximum values, respectively. Horizontal lines superimposed to the violins indicate means.

To estimate how muscle activity and activation changed as a function of body pitch angle (rotation about the transverse axis), we fitted a logistic function (Eqn. 1) to the data.

$$f(x) = \frac{\gamma}{1 + e^{\beta(x-\alpha)}} + \delta \qquad \text{(Eqn. 1)}$$

To estimate how swing and stance duration changed with forward velocity, we fitted a linear ($f(x) = \alpha x + \beta$) and hyperbolic ($f(x) = \alpha/x$) function to the data, respectively. Fit parameters α, β, γ, and, δ were estimated using an iterative, non-linear least-squares approach, using the MATLAB function fit(). Statistical inference was based on bootstrap randomization tests with $B = 10^8$ samples. For this, we determined the probability p of observing that a statistical summary of the permutated test statistic $T*$ is more extreme than the test statistic T of the measured samples (Mackinnon, 2009; Eqn. 2).

$$p = \frac{1}{B} \sum_{b=1}^{B} T^* \geq T \qquad \text{(Eqn. 2)}$$

To detect differences among the seven step categories, response variables with their step category labels were ranked separately for each of the $n = 9$ animals. With the $k = 9$ dependent step categories, we used Friedman's test statistic (Friedman, 1937; Eqn. 3) for a ranked consistency test on the mean ranks r per step category. For the permutated test statistic (Eqn. 2), ranks were formed based on random samples (with replacement) from all animals and step categories.

$$T_{ranked} = \frac{12n}{k(k+1)} \sum_{j=1}^{k} \left(r_j - \frac{k+1}{2} \right)^2 \qquad \text{(Eqn. 3)}$$

The test statistic used for a two-sample, two-tailed comparison of observation z (mean $\bar{z}$, standard deviation σ_z, sample size n) and observation y (mean $\bar{y}$, standard deviation σ_y, sample size m) is given below (Eqn. 4). Here, bootstrap samples were drawn from a joint distribution of z and y with the first n samples assigned to z* and the remaining m samples to y*.

$$T_{two-sample} = \frac{|\bar{z} - \bar{y}|}{\sqrt{\sigma_z^2/n + \sigma_y^2/m}} \qquad \text{(Eqn. 4)}$$

The test statistic used for a one-sample, two-tailed comparison of observation z (mean $\bar{z}$, standard deviation σ_z, sample size n), that compares the mean of the sample with a pre-determined value μ_0, *e.g.* 0.5, is given in the following equation (Eqn. 5). Bootstrap samples were drawn from the empirical distribution $\tilde{z}_i = z_i - \bar{z} + \mu_0, i = 1, \dots, n$.

$$T_{one-sample} = \frac{|\bar{z} - \mu_0|}{\sigma_z/\sqrt{n}} \qquad \text{(Eqn. 5)}$$

We complement reports of *p*-values with corresponding *s*-values (Shannon information, Eqn. 6) to portray evidential value better, as it is expressed in bits of information against the tested hypothesis (as suggested in Wasserstein et al., 2019).

$$s = -log_2(p) \qquad \text{(Eqn. 6)}$$

Note that by definition, this method yields a lowest achievable *p*-value of $1/B = 10^{-8}$ and thus a Shannon information of 26 bits. Effect sizes were estimated by the standardized difference between two means (Cohen's *d*).

Data and code availability

The data supporting this study's findings and the code used for analysis are available from the corresponding author upon reasonable request.

RESULTS

To gain insight into adaptive motor control, unrestrained walking stick insects were recorded as they encountered a step-change in walkway slope (±45°), causing change in load distribution among legs. In total, $n = 990$ steps from $N = 9$ animals were collected across all step categories (see Table 1 for numbers for each category). In the following sections, we will first analyze how the change in load distribution affects hind leg muscle activity and kinematics. In particular, we will analyze how this relates to load-dependent regulation of joint stiffness by estimating the co-activation of antagonistic muscles. Finally, we will connect our findings on the transition between two steady states to transient modulation of muscle activity in response to destabilizing lift-off events of neighboring legs or overall unloading of legs during crawling.

Muscle activity was strongly affected by a step-change in walkway slope

Muscle activity showed substantial inclination-dependent changes during the transition from level to slope walking. Differences between step categories were visible already in raw EMG traces (Fig. 2A & B; Movies 1-2). During swing movements, the motoneuronal drive to the retractor was independent of the step category ($p = 0.24$, $s = 2$; ranked consistency randomization test; Fig. 2C$_i$). However, during stance movements the motoneuronal drive was modulated by the step category ($p = 10^{-8}$, $s = 26$; ranked consistency randomization test), with activity increasing with increasing inclination (Fig. 2C$_{ii}$). Effects between consecutive step categories were on average small ($d = 0.2$), indicating gradual changes. Yet, they added up to a very large effect when comparing steady-state downwards with upwards walking ($d = 1.2$, $p = 0.007$, $s = 7$; two-sample two-tailed randomization test). At the same time, the protractor received strong motoneuronal drive during swing movements (Fig. 2D$_i$), reflecting the forward movement of the leg. The spike rate was modulated by the step category ($p = 10^{-8}$, $s = 26$; ranked consistency randomization test) with, on average, minor effects between consecutive step categories ($d = 0.4$) that add up to a large effect ($d = 1.4$) when comparing steady-state downwards with upwards walking ($p = 6.8*10^{-4}$, $s = 10$; two-sample two-tailed randomization test). For stance movements, the drive to the protractor was also modulated by the step category ($p = 10^{-8}$, $s = 26$; ranked consistency randomization test) with activity decreasing with increasing inclination (Fig. 2D$_{ii}$). Again, this modulation changed gradually (mean $d = 0.6$) and eventually added up to a substantial effect ($d = 1.8$) when comparing the two categories of steady-state slope walking ($p = 6.2*10^{-6}$, $s = 17$; two-sample two-tailed randomization test). Altogether, the activity of both

muscles, retractor and protractor, was modulated gradually as the animal experienced a transition in load distribution in conjunction with a step-change in slope.

To further illustrate this load-dependent modulation of muscle activity throughout the step cycle, we used rectified and smoothed EMG traces normalized to the mean duration of swing and stance phases (Fig. 3A). For the transition from level to upslope walking, retractor muscle activity during stance increased gradually with each subsequent leg on the incline, whereas it gradually decreased during the transition from level to downslope walking (Fig. 3A$_i$). Along with a change in magnitude, the time of the maximum activity gradually shifted to an earlier part of the stance movement during an upslope transition and to a later part during a downslope transition. This was different for the protractor. There, muscle activity during stance was strongest during steady-state downward walking, intermediate for level walking, and diminished during upward walking (Fig. 3A$_{ii}$). During swing movements, *i.e.*, when the hind leg was not mechanically coupled to its neighboring legs through the ground, protractor activity still showed inclination-dependent modulation. With each leg stepping onto a downward slope, the magnitude of protractor activity decreased gradually, whereas it increased gradually as the animal stepped onto the upward slope.

As a proxy for joint stiffness at the thorax-coxa joint, we estimated the degree of co-contraction of the two antagonist muscles. In a first step to do so, we calculated the time course of muscle activation of both muscles using the non-linear Hatze-Zakotnik model of insect muscle activation dynamics (Zakotnik et al., 2006; Harischandra et al., 2019). This model takes account of the long time constants of single twitches in insect muscle and non-linear force potentiation for spike frequencies between 10 Hz and 30 Hz. The mean and 95% confidence bands of the estimated muscle activation time courses are shown (Fig. 3B & C). Muscle activation of the retractor (Fig. 3B$_i$) showed essentially the same inclination-dependent modulation as found for retractor muscle activity (Fig. 3A$_i$). Yet, the curves of Figure 3B were generally not as steep as their counterparts in Fig. 3A. This can be attributed to the long time constants of insect muscle activation dynamics. During stance, maximum retractor activation increased gradually during the upslope transition, whereas it decreased gradually during the downslope transition. On the other hand, protractor activation during stance was highest for steady-state downward walking, intermediate for level walking, and diminished in the second half of stance during upward walking (Fig. 3B$_{ii}$). Again, time courses of transition steps of either walking condition resembled intermediates of the steady states between which they occurred.

Taken together, these results suggest that muscle activation of the two antagonists that protract/retract the hind leg about the ThC joint is subject to strong, inclination-dependent modulation.

Changes in co-contraction of antagonistic muscles

Since both retractor and protractor muscles were active during level walking, and the slope-dependent changes in the activity of both muscles were similar, though with opposing sign, both neural co-activity and muscular co-activation of antagonists appeared to be important parameters in this paradigm. The most salient slope-dependent changes in muscle activity occurred during the first half of the stance movement (Fig. 3), reflecting previous reports on the biphasic nature of stick insect stance movements with an early support part (Graham, 1983). Therefore, only the first half of the step cycle was evaluated further. To do so, protractor activity was subtracted from retractor activity. The corresponding average time courses are shown in Fig. 4A$_i$. The difference in muscle activity depended strongly on step category ($p = 10^{-8}$, $s = 26$; ranked consistency randomization test). Already the first transition step, *i.e.*, with only the front leg on the incline, was clearly distinguishable from level walking. The difference in muscle activity strongly changed in favor of the retractor during the upward transition, and in favor of the protractor during the downward transition ($p_{up1} = 0.053$, $s_{up1} = 4$, $d_{up1} = 0.9$, $p_{dwn1} = 0.011$, $s_{dwn1} = 6$, $d_{dwn1} = 1.1$; two-sample two-tailed randomization test). With each subsequent leg on the slope, the difference between both muscles increased gradually in the respective direction. The graded change in the pattern of muscle activity throughout the traversal was strongly correlated with a change in body pitch relative to gravity ($r^2 = 0.97$, logistic regression; Fig. 4A$_{ii}$). With regard to our proxy for joint stiffness, we found a similarly strong correlation between the difference in muscle activation and a change in body pitch relative to gravity ($p = 10^{-8}$, $s = 26$; ranked consistency randomization test; Fig. 4B$_{ii}$). Although the effect size of the step towards the slope was smaller ($d_{up1} = 0.9$; $d_{dwn1} = 0.5$), the eventual steady-state difference was of a similar magnitude.

Kinematic parameters were barely affected by a step-change in walkway slope

Hind leg kinematics were recorded in synchrony with antagonistic muscle activity. To evaluate potential kinematic adjustments in response to a step-change in walkway slope and the resulting change in mechanical demand, we compared kinematic parameters during level walking with those during steady-state slope walking and the transition strides in-between.

With walking speeds ranging from 13.6 mm/s to 81.3 mm/s (38.2 ± 10.6 mm/s; mean ± s.d.), animals readily transitioned from level to slope walking (Fig. 5A). As in previous studies (for review, see Dürr et al., 2018) hind leg stance duration decreased hyperbolically with increasing speed, irrespective of step category (Fig. 5B$_i$). At the same time, the duration of swing movements remained nearly unaffected (Fig. 5B$_{ii}$).

As in our previous study (Dallmann et al., 2019), joint angle time courses were very similar across steady-state conditions (Fig. 5C$_i$ & C$_{ii}$). The hind leg was flexed, levated, supinated, and protracted during swing movements, whereas it was extended, depressed, pronated, and retracted during stance movements. The only joint that changed movement direction before the swing-to-stance transition was the coxa-trochanter joint. In all three steady-state conditions, the switch from levation to depression occurred before the onset of stance because depression must precede touch-down which, in turn, must precede the onset of stance. When comparing step categories during the transition to slope walking, it was this depression in late swing that differed most noticeably from level walking, along with the subsequent depression in early stance. During the transition, the coxa-trochanter joint angle depressed more strongly during the upward transition (Fig. 5C$_i$) and depressed less strongly during the downward transition (Fig. 5C$_{ii}$). Fig. 5C$_{iii}$ illustrates these changes of the mean differences in coxa-trochanter angle compared to level walking at 25 % of the step cycle (dotted lines in Fig. 5C$_i$ & C$_{ii}$). The difference to level walking was strongest for the third transition step during the upward transition ($p = 6.3*10^{-4}$, $s = 10$, $d = 1.75$; one-sample two-tailed randomization test) and for the second transition step during the downward transition ($p = 0.002$, $s = 9$, $d = 1.66$; one-sample two-tailed randomization test). Afterwards, the deviation decreased and approached the value during level walking. The slope-dependent differences in other joint angle time courses were not nearly as strong as that in levation of the coxa-trochanter joint. As described by the preceding paper (Dallmann et al., 2019), the hind leg tended to be flexed less and protracted more in early stance during the upward transition and pronated more strongly throughout the entire stance movement. During the downward transition, extension and supination joint angles were mainly within the 95 % confidence intervals for level walking. An exception was the protraction of the thorax-coxa joint during early stance movement, which tended to be smaller. The mentioned change in protraction joint angle around the time of the swing-stance transition was consistent with a change in the anterior-posterior touch-down position ($p = 10^{-8}$, $s = 26$; ranked consistency randomization test; Fig. 5D).

Taken together, these results suggest that kinematic parameters were affected only little by a step-change in walkway slope and the corresponding shift in load distribution.

Transient changes in muscle activity after destabilizing events of neighboring legs

During walking, the stepping rhythm of each leg implies rhythmic load transfer among legs. That is, additionally to the change in load as a result of the change in inclination, each lift-off event of a leg induces mechanical load transfer to its neighboring legs. This is why we analyzed how muscle activity in the right hind leg (R3) was modulated in response to lift-off of its nearest neighbors: the ipsilateral right middle leg (R2) and the contralateral left hind leg (L3). To do so, we considered all lift-off events

that occurred while R3 was in stance and, therefore, mechanically coupled with all other legs that had ground contact.

During level walking, retractor activity of R3 decreased within approx. 100 ms after the ipsilateral middle leg R2 had lifted off (black area in Fig. 6A$_i$). For the protractor, the opposite was true with an immediate increase of activity (black area in Fig. 6A$_{ii}$). Note that this transient response follows the same pattern observed for the downward transition (Fig. 6A and 4A, blue traces), *i.e.*, shifting the difference between protractor and retractor activity in favor of the protractor. During steady-state walking on either slope, neither muscle showed consistent, event-related activity changes upon lift-off of R2 (magenta and blue shaded areas in Fig. 6A). Muscle activity during transition steps was intermediate between these steady-state response types and gradually approached the steady-state situation on the slope with each subsequent leg on the incline.

In contrast, lift-off events of the contralateral hind leg L3 had the opposite effect on retractor and protractor activity of R3 during level walking (Fig. 6B). Upon lift-off of L3, protractor activity of R3 declined rapidly, whereas retractor activity increased (black areas in Fig. 6B). Note that this response to lift-off events follows the same pattern observed for the upward transition (Fig. 3A and 4A, magenta traces), *i.e.*, shifting the difference between protractor and retractor activity in favor of the retractor. As for lift-off of R2, lift-off of L3 was followed by no pronounced, transient change in activity of either muscle during steady-state slope walking. Muscle activity during transition steps (magenta and blue lines in Fig. 6B) was intermediate between the steady states.

In summary, both retractor and protractor muscle activity revealed transient, event-related changes to destabilizing lift-off events of neighboring legs and an associated change in load distribution during level walking. Both kinds of transient destabilizations were consistently followed by a transient reduction of co-activation of antagonistic muscles. This hints at a common principle underlying both transient and persistent changes in muscle activity patterns, regardless of whether the disturbance in load distribution was caused by a change in pitch relative to gravity or by a destabilizing lift-off event of a neighboring leg.

No co-activation of antagonistic muscles during crawling

Yet another change in load distribution occurs whenever the legs do not suspend the body above the ground, such that the animal is effectively crawling rather than walking. In all analyses presented so far, steps were excluded if the thorax was in contact with – and sliding along – the ground. In the following, we will use the term crawling for this type of locomotion (as opposed to walking, where only the feet are in contact with the ground). Crawling occurred occasionally and was typically attributed to fatigue at the end of a long recording session. In the case of one animal, we were able to conduct a systematic within-session comparison between crawling as opposed to regular walking.

This animal crawled for several trials in the middle of the recording session, with regular walking trials before and after this crawling episode. Thus, we could compare regular level walking steps before ($n = 7$) and after ($n = 8$) thoracic ground contact with those when the animal crawled ($n = 4$) (Fig. 7). Representative side-view images (Fig. 7A$_i$ & A$_{iii}$) and corresponding average joint angle time courses (Fig. 7B, black solid and dotted lines) show that the regular walking posture was maintained before and after the crawling episode. Also, raw EMG recordings and time courses of the relative retractor and protractor activity before and after crawling were broadly similar (Fig. 7C & D, solid and dotted black lines). In contrast, they differed markedly during crawling (Fig. 7C & D, green lines).

Crawling affected joint angle time courses and antagonistic muscle activity of the right hind leg substantially. Compared with regular walking steps, the leg was persistently more levated, flexed, and protracted throughout the step. Solely the supination of the leg plane stayed nearly unaffected. The examples of raw EMG traces during crawling (Fig. 7C$_{ii}$) were similar to those observed during steady-state upward walking (Fig. 2A), with protractor activity restricted to the swing movement. Relative muscle activity profiles (Fig. 7D) further revealed that protractor activity during swing movements was decreased, while retractor activity during stance movements was slightly increased during crawling.

Furthermore, the successful recovery of body posture and muscle activity after crawling revealed that co-activation of antagonistic muscles re-occurred only as the hind leg contributed to carrying the load of the body again, but not while the body was "supported" by the ground. This suggests that co-contraction of retractor and protractor muscles may act to counter gravity-induced collapse, *i.e.*, the effort of the animal to maintain balance with the body suspended above the ground.

DISCUSSION

Here, we provide three-fold evidence for a fast and flexible mechanism to achieve resilience to both transient and sustained changes in load distribution that is based on continuous regulation of antagonist muscle co-activation in unrestrained moving stick insects. In a previous study, we showed that persistent changes in load distribution – as caused by a change in body orientation relative to gravity – lead to substantial changes in joint torques and muscle activity, with very little change in limb kinematics (Dallmann et al., 2019). First, we replicate numerous of these findings. We show that the transition between two steady states that differ in load distribution is characterized by a gradual change in muscle activity (Fig. 2) and muscle activation (Fig. 3), with antagonist muscle co-activation following a monotonous function of body orientation relative to gravity (Fig. 4), and small, primarily transient changes in limb kinematics (Fig. 5). Second, we demonstrate that the same changes in antagonist co-activation occur in response to highly transient changes in load distribution after de-

stabilizing lift-off events of neighboring legs (Fig. 6). Third, we show that a state-dependent change in load distribution during crawling (as opposed to walking) reversibly abolishes antagonist muscle co-activity (Fig. 7). Given the consistency of these three load-induced adjustments of antagonist muscle co-activity, we argue that stick insects respond to both transient and sustained changes in load distribution by continuous regulation of antagonist muscle co-activation and, therefore, regulation of muscle co-contraction and joint stiffness.

Muscle co-contraction and joint stiffness

The significance of joint stiffness as a control variable in mammals has been established for a long time in sensorimotor physiology (*e.g.*, Houk, 1979), biomechanics (*e.g.*, Günther and Blickhan, 2002; Blickhan et al., 2007), and computational motor control (*e.g.*, Franklin and Wolpert, 2011). Indeed, the regulation of stiffness in limb movement control must have evolved independently in all three remaining taxa of limbed animals (Arthropoda, Cephalopoda, Tetrapoda) as their last common ancestors did not have limbs. Representative examples include load compensation in targeted movements in an arthropod limb (locust: Matheson and Dürr, 2003; Zakotnik et al., 2006; Page et al., 2008), the temporary formation of quasi-rigid links in goal-directed movements of a cephalopod limb (octopus: Sumbre et al., 2006; Yekutieli et al., 2007), and the control of grasping precision in a tetrapod limb (human: De Serres and Milner, 1991; Gribble et al., 2003). Similarly, variable stiffness control has gained much attention in robotics (for review, see Wolf et al., 2016)

Owing to the non-linear properties of muscle contraction dynamics, a pair of antagonistic muscles allows for independent control of joint position and stiffness, with antagonist co-activation being key for controlling joint stiffness (Bührmann and Di Paolo, 2006). Due to the long activation and deactivation time constants of insect muscles (Bässler and Stein, 1996; Hooper et al., 2007), our finding of load-dependent adjustment of antagonist co-activity implies that stick insects regulate a variable related to muscle co-activation. As muscle activation determines isometric contraction force (*e.g.*, Harischandra et al., 2019), muscle co-activation translates into isometric co-contraction and, therefore, the resistance of the actuated joint against deflection, *i.e.*, joint stiffness. Comparing the estimated characteristic of antagonist co-activation on body pitch (Fig. 4B$_{ii}$) with that of co-activity (Fig. 4A$_{ii}$), muscle activation dynamics prove to have a linearizing effect. For level walking, when both the retractor and protractor were active throughout the stance movement (Fig. 3), thorax-coxa (ThC) joint stiffness was the largest. Yet, in the case of body pitch changing in either direction relative to gravity, ThC joint stiffness decreased through an increasing bias towards activating of one ThC joint muscle only.

Note that we do not measure muscle co-contraction or joint stiffness directly, but infer it from estimates of muscle co-activation, *i.e.*, the degree of "neural drive" to both muscles actuating the ThC joint. This indirect estimate neglects any differences between retractor and protractor muscles and lever arms. Since we find very little slope-dependent change in joint kinematics, but strong slope-dependent change in muscle co-activation, our conclusion of slope-dependent change in co-contraction and joint stiffness is justified qualitatively. Nevertheless, further research will be necessary to provide a quantitative estimate of joint stiffness, as this requires knowledge of the underlying muscle and joint geometries.

Our finding reflects the persistent changes in load distribution and altered mechanical demand at the ThC joint for either propulsion (upward walking), stability of body posture (level walking), or braking (downward walking). Co-contraction of coxal muscles has also been reported for freely walking locusts (Duch and Pflüger, 1995), which alter their muscular activity patterns to cope with different conditions, such as vertical climbing or upside-down walking. Adjustments of muscle co-contraction due to changing mechanical demand, *e.g.*, a change in load, were further evaluated by Zakotnik *et al.* (2006) on locust hind leg extensor and flexor tibiae muscles. By expanding on the dynamic range of joint torques, they found that net joint torques can be increased substantially by rather small changes in muscle force, provided that the normal movement involved sufficient co-contraction.

Load-dependent muscle activation and the control of stance

In line with several earlier studies, we observed the most salient changes in the first half of the stance movement, corroborating the concept of a biphasic stance movement with an early support and a later propulsive part (cockroach: Krauthamer and Fourtner, 1978; Larsen et al., 1995; stick insect: Graham, 1983). Similarly, our results on protractor activity agree with previous experiments revealing braking activity during the early part of this movement (Graham and Wendler, 1981). The phasic nature of load-dependent effects on stance muscle activation supports the view of a reflexive control of limb posture, resulting in relatively small changes in spatial and temporal kinematic parameters (Fig. 5). Similarly, seed-harvesting ants do not employ different locomotor behaviors when carrying loads but use their hind legs to cling to the ground (Merienne et al., 2020). We conclude that insects from different orders regulate limb posture by adjusting muscle activation in response to changes in load distribution.

Compared with such persistent changes in load distribution, transient load transfer to the hind leg after lift-off of the anterior or contralateral neighbor leg increases the mechanical demand at the ThC joint to stabilize posture. Owing to its vicinity to the center of mass (CoM), the ThC joint of the hind leg needs to be stabilized with opposite sign, depending on whether the ipsilateral middle leg (anterior to the CoM) or contralateral hind leg (posterior to the CoM) lifts off. The reflexive nature of

this response is typically attributed to sensory feedback from campaniform sensilla (CS), which are known for their important role in postural control and walking (reviewed by Zill et al., 2004; Tuthill and Wilson, 2016). The discharges of CS depend upon their location (*e.g.*, Haberkorn et al., 2019), the orientation of their long axis (Spinola and Chapman, 1975), and the vectoral direction of the imposed or self-generated forces (*e.g.*, Zill et al., 2012). This implies that a change in body orientation relative to gravity will affect the overall distribution of CS activity. In the case of muscle activity at the ThC joint, as investigated here, trochanteral CS are known to be part of feedback loops that minimize imposed strains in the leg during standing and walking (Schmitz, 1993; Schmitz and Stein, 2000). CS ablations revealed that load-dependent activation of retractor and protractor muscles of the ThC joint are mainly driven by trochanteral CS, although CS from more distal leg parts may modulate retractor activity (Haberkorn et al., 2019). Furthermore, the neural processing of trochanteral CS depends on walking direction and is sufficient to trigger the transition from stance to swing in both forward and backward walking animals (Akay et al., 2004, 2007).

This body of evidence strongly suggests that the three kinds of changes in load distribution tested here must have affected load encoding of trochanteral CS and, as a consequence, retractor and protractor motoneuron activity. Yet, we cannot rule out additional effects of other CS groups (*e.g.*, femoral CS group 5; see Haberkorn et al., 2019), indirect contributions and/or interaction of CS activity from legs other than the hind leg recorded, nor the influence of other sensory signals (*e.g.*, contact information). Given the complexity of CS effects in stationary animals with highly controlled stimuli (Haberkorn et al., 2019) and the encoding of loading and unloading (Ridgel et al., 1999), a systematic investigation of CS effects on muscle co-contraction in free walking animals is clearly beyond the scope of the present study. Future research will need to address both the interplay of several CS groups and the up- and down-regulation of antagonistic muscle activity in freely walking insects.

As a neuromuscular strategy, co-contraction of antagonistic muscles has also been identified for mammals that transition between slopes (Gottschall and Nichols, 2011). Here, changes in muscle activity were reported to correspond mostly with modifications of head pitch. The integration of vestibular information with information from neck proprioceptors could be used to estimate body orientation with respect to gravity. Notably, humans adjust muscle activity and head pitch already in anticipation of the slope, but only if the upcoming disturbance has not been camouflaged (Müller et al., 2015). This could be explained by the fast speed of humans and the fact that bipedal locomotion demands distinct anticipation and transition steps (Gottschall and Nichols, 2011). We did not observe distinct transition steps in our study, and potentially a six-legged walker with low speed and low inertia does not need to anticipate disturbances. In principle, stick insects could use their long antennae to perceive relative changes in the direction of the gravity vector (Wendler, 1965; Bässler,

1971), although walking *C. morosus* only rarely touch the ground with their antennae. Future work may address the contribution of antennal graviception to the observed changes in leg muscle co-contraction.

Motor patterns with and without load

Last but not least, our third example addressed state-dependent changes in load distribution during crawling, where antagonist muscle activity was strictly alternating without co-activity (Fig. 7C & D). We argue that the transfer of load from the legs to the main body implies that the legs need no longer counteract gravity-induced collapse through increased joint stiffness, making costly co-contraction of antagonistic muscles dispensable.

Our results on state-dependent protractor-retractor co-contraction during level walking and crawling are in line with studies using three different experimental contexts. Whereas the maintained antagonist co-activity during walking (Fig. 7C$_i$, C$_{iii}$, D, E) replicates the findings by Dallmann *et al.* (2019), our results on crawling are the same as those obtained from supported walking animals in that antagonist muscle activity was strictly reciprocal (treadmill: Akay et al., 2004; slippery surface: Rosenbaum et al., 2010). Supported-walking paradigms (treadmill; slippery surface) and crawling have in common that the animal does not support its body weight and, therefore, does not need to stabilize the body against gravity-induced collapse. We conclude that our results in Fig. 7 could resolve an apparent discrepancy in the literature by highlighting the significance of the acting load distribution on the generation of rhythmic motor patterns. While this conclusion is consistent with current knowledge about sensorimotor effects of changes in load (see the previous section), future research on the sensory modulation of muscle co-contraction will need to test for potential effects of body contact as it occurs during crawling and supported-walking paradigms.

Conclusion

Resilience to sudden changes in substrate properties is crucial for terrestrial locomotion when navigating through variable environments. Our study provides three-fold evidence on adjustments of antagonist muscle activity in response to a change in load distribution. We conclude that both persistent (though graded) and transient adjustments of antagonist muscle co-contraction follow the same load-dependent and continuous pattern during the first half of the stance phase. While further research will need to address how local pre-motor and motor networks integrate local load feedback to up- or down-regulate activity of both antagonistic muscles, our results clearly suggest a common mechanism underlying both transient and persistent regulation of antagonist co-contraction and, thus, joint stiffness.

COMPETING INTERESTS

The authors declare no competing or financial interests.

AUTHOR CONTRIBUTIONS

JS, YG, and VD designed the study; JS established the setup; YG conducted the experiments, analyzed the data, generated all figures, and drafted the manuscript; VD and JS supervised YG; YG and VD wrote the paper.

REFERENCES

Akay T, Haehn S, Schmitz J, Büschges A (2004) Signals from load sensors underlie interjoint coordination during stepping movements of the stick insect leg. J Neurophysiol 92:42–51.

Akay T, Ludwar BC, Goritz ML, Schmitz J, Büschges A (2007) Segment specificity of load signal processing depends on walking direction in the stick insect leg muscle control system. J Neurosci 27:3285–3294.

Bässler U (1971) Zur Bedeutung der Antennen für die Wahrnehmung der Schwerkraftrichtung bei der Stabheuschrecke Carausius morosus. Kybernetik 9:31–34.

Bässler U, Stein W (1996) Contributions of structure and innervation pattern of the stick insect extensor tibiae muscle to the filter characteristics of the muscle-joint system. J Exp Biol 199:2185–2198.

Blickhan R, Seyfarth A, Geyer H, Grimmer S, Wagner H, Günther M (2007) Intelligence by mechanics. Philos Trans R Soc A Math Phys Eng Sci 365:199–220.

Bührmann T, Di Paolo E (2006) Biological actuators are not just springs investigating muscle dynamics and control signals. In: Nolfi (Ed.) From Animats to Animals 9. International Conference on Simulation of Adaptive Behavior, pp 89–100.

Cruse H (1976) The function of the legs in the free walking stick insect, Carausius morosus. J Comp Physiol A 112:235–262.

Dallmann CJ, Dürr V, Schmitz J (2016) Joint torques in a freely walking insect reveal distinct functions of leg joints in propulsion and posture control. Proc R Soc B Biol Sci 283:20151708-.

Dallmann CJ, Dürr V, Schmitz J (2019) Motor control of an insect leg during level and incline walking. J Exp Biol 222:jeb188748.

Dallmann CJ, Hoinville T, Dürr V, Schmitz J (2017) A load-based mechanism for inter-leg coordination in insects. Proc R Soc B Biol Sci 284:1–9.

Duch C, Pflüger HJ (1995) Motor patterns for horizontal and upside down walking and vertical climbing in the locust. J Exp Biol 198:1963–1976.

Dürr V, Theunissen LM, Dallmann CJ, Hoinville T, Schmitz J (2018) Motor flexibility in insects: adaptive coordination of limbs in locomotion and near-range exploration. Behav Ecol Sociobiol 72:15.

Ekeberg O, Pearson K (2005) Computer simulation of stepping in the hind legs of the cat: An examination of mechanisms regulating the stance-to-swing transition. J Neurophysiol 94:4256–4268.

Franklin DW, Wolpert DM (2011) Computational mechanisms of sensorimotor control. Neuron 72:425–442. http://dx.doi.org/10.1016/j.neuron.2011.10.006.

Friedman M (1937) The use of ranks to avoid the assumption of normality implicit in the analysis of variance. J Am Stat Assoc 32:675–701.

Full RJ, Tullis A (1990) Energetics of Ascent : Insects on Inclines. J Exp Biol 317:307–317.

Gottschall JS, Nichols TR (2011) Neuromuscular strategies for the transitions between level and hill surfaces during walking. Philos Trans R Soc B Biol Sci 366:1565–1579.

Graham D (1983) Insects are both impeded and propelled by their legs during walking. J Exp Biol 137:129–137.

Graham D, Wendler G (1981) Motor output to the protractor and retractor coxae muscles in stick insects walking on a treadwheel. Physiol Entomol 6:161–174.

Gregor RJ, Smith DW, Prilutsky BI (2006) Mechanics of slope walking in the cat: Quantification of muscle load, length change, and ankle extensor EMG patterns. J Neurophysiol 95:1397–1409.

Gribble PL, Mullin LI, Cothros N, Mattar A (2003) Role of cocontraction in arm movement accuracy. J Neurophysiol 89:2396–2405.

Günther M, Blickhan R (2002) Joint stiffness of the ankle and the knee in running. J Biomech 35:1459–1474.

Haberkorn A, Gruhn M, Zill SN, Büschges A (2019) Identification of the origin of force-feedback signals influencing motor neurons of the thoraco-coxal joint in an insect. J Comp Physiol A 205:253–270. https://doi.org/10.1007/s00359-019-01334-4.

Harischandra N, Clare AJ, Zakotnik J, Blackburn LML, Matheson T, Dürr V (2019) Evaluation of linear and non-linear activation dynamics models for insect muscle. PLoS Comput Biol 15:1–30.

Hooper SL, Guschelbauer C, Uckermann G, Büschges A (2007) Slow temporal filtering may largely explain the transformation of stick insect (Carausius morosus) extensor motor neuron activity into muscle movement. J Neurophysiol 98:1718–1732.

Houk JC (1979) Regulation of stiffness by skeletomotor reflexes. Annu Rev Physiol 41:99–114.

Krauthamer V, Fourtner CR (1978) Locomotory activity in the extensor and flexor tibiae of the cockroach, Periplaneta americana. J Insect Physiol 24:813–819.

Larsen G. S, Frazier SF, Fish SE, Zill SN (1995) Effects of load inversion in cockroach walking. J Comp Physiol A Neuroethol Sensory, Neural, Behav Physiol 176:229–238.

Lay AN, Hass CJ, Nichols TR, Gregor RJ (2007) The effects of sloped surfaces on locomotion: An electromyographic analysis. J Biomech 40:1276–1285.

Mackinnon JG (2009) Bootstrap hypothesis testing. Handb Comput Econom:183–213.

Mendes CS, Rajendren S V., Bartos I, Márka S, Mann RS (2014) Kinematic responses to changes in walking orientation and gravitational load in drosophila melanogaster. PLoS One 9.

Merienne H, Latil G, Moretto P, Fourcassié V (2020) Walking kinematics in the polymorphic seed harvester ant Messor barbarus: Influence of body size and load carriage. J Exp Biol 223.

Müller R, Häufle DFB, Blickhan R (2015) Preparing the leg for ground contact in running: The contribution of feed-forward and visual feedback. J Exp Biol 218:451–457.

Noah AJ, Quimby L, Frazier FS, Zill SN (2001) Force detection in cockroach walking reconsidered: Discharges of proximal tibial campaniform sensilla when body load is altered. J Comp Physiol - A Sensory, Neural, Behav Physiol 187:769–784.

Owaki D, Goda M, Miyazawa S, Ishiguro A (2017) A minimal model describing hexapedal interlimb coordination: The tegotae-based approach. Front Neurorobot 11:1–13.

Owaki D, Kano T, Nagasawa K, Tero A, Ishiguro A (2013) Simple robot suggests physical interlimb communication is essential for quadruped walking. J R Soc Interface 10.

Page KL, Zakotnik J, Dürr V, Matheson T (2008) Motor control of aimed limb movements in an insect. J Neurophysiol 99:484–499.

Ridgel AL, Frazier SF, Dicaprio RA, Zill SN (1999) Active signaling of leg loading and unloading in the cockroach. J Neurophysiol 81:1432–1437.

Ridgel AL, Frazier SF, DiCaprio RA, Zill SN (2000) Encoding of forces by cockroach tibial campaniform sensilla: Implications in dynamic control of posture and locomotion. J Comp Physiol - A Sensory, Neural, Behav Physiol 186:359–374.

Rosenbaum P, Wosnitza A, Büschges A, Gruhn M (2010) Activity patterns and timing of muscle activity in the forward walking and backward walking stick insect Carausius morosus. J Neurophysiol 104:1681–1695.

Schmitz J (1993) Load-Compensating Reactions in the Proximal Leg Joints of Stick Insects During Standing and Walking. J Exp Biol 33:15–33.

Schmitz J, Stein W (2000) Convergence of load and movement information onto leg motoneurons in insects. J Neurobiol 42:424–436.

Seidl T, Wehner R (2008) Walking on inclines: How do desert ants monitor slope and step length. Front Zool 5:1–15.

Spinola SM, Chapman KM (1975) Proprioceptive indentation of the campaniform sensilla of cockroach legs. J Comp Physiol A 96:257–272.

Sumbre G, Fiorito G, Flash T, Hochner B (2006) Octopuses sse a human-like dtrategy to control precise point-to-point arm movements. Curr Biol 16:767–772.

Szczecinski NS, Bockemühl T, Chockley AS, Büschges A (2018) Static stability predicts the continuum of interleg coordination patterns in Drosophila. J Exp Biol 221.

Theunissen LM, Dürr V (2013) Insects use two distinct classes of steps during unrestrained locomotion. PLoS One 8:1–18.

Tuthill JC, Wilson RI (2016) Mechanosensation and adaptive motor control in insects. Curr Biol 26:R1022–R1038. http://dx.doi.org/10.1016/j.cub.2016.06.070.

Wasserstein RL, Schirm AL, Lazar NA (2019) Moving to a world beyond "p< 0.05." Am Stat 73:1–19.

Weihmann T, Blickhan R (2009) Comparing inclined locomotion in a ground-living and a climbing ant species: Sagittal plane kinematics. J Comp Physiol A 195:1011–1020.

Wendler G (1965) Über den Anteil der Antennen an der Schwererezeption der Stabheuschrecke Carausius morosus Br. Z vgl Physiol 51:60–66.

Wolf S, Grioli G, Eiberger O, Friedl W, Grebenstein M, Hoppner H, Burdet E, Caldwell DG, Carloni R, Catalano MG, Lefeber D, Stramigioli S, Tsagarakis N, Van Damme M, Van Ham R, Vanderborght B, Visser LC, Bicchi A, Albu-Schaffer A (2015) Variable stiffness actuators: Review on design and components. IEEE/ASME Trans Mechatronics 21:2418–2430.

Yekutieli Y, Mitelman R, Hochner B, Flash T (2007) Analyzing octopus movements using three-dimensional reconstruction. J Neurophysiol 98:1775–1790.

Zakotnik J, Matheson T, Dürr V (2006) Co-contraction and passive forces facilitate load compensation of aimed limb movements. J Neurosci 26:4995–5007.

Zill SN, Keller BR, Duke ER (2009) Sensory signals of unloading in one leg follow stance onset in another leg: Transfer of load and emergent coordination in cockroach walking. J Neurophysiol 101:2297–2304.

Zill SN, Schmitz J, Büschges A (2004) Load sensing and control of posture and locomotion. Arthropod Struct Dev 33:273–286.

Zill SN, Schmitz J, Chaudhry S, Büschges A (2012) Force encoding in stick insect legs delineates a reference frame for motor control. J Neurophysiol 108:1453–1472.

Figures and Tables
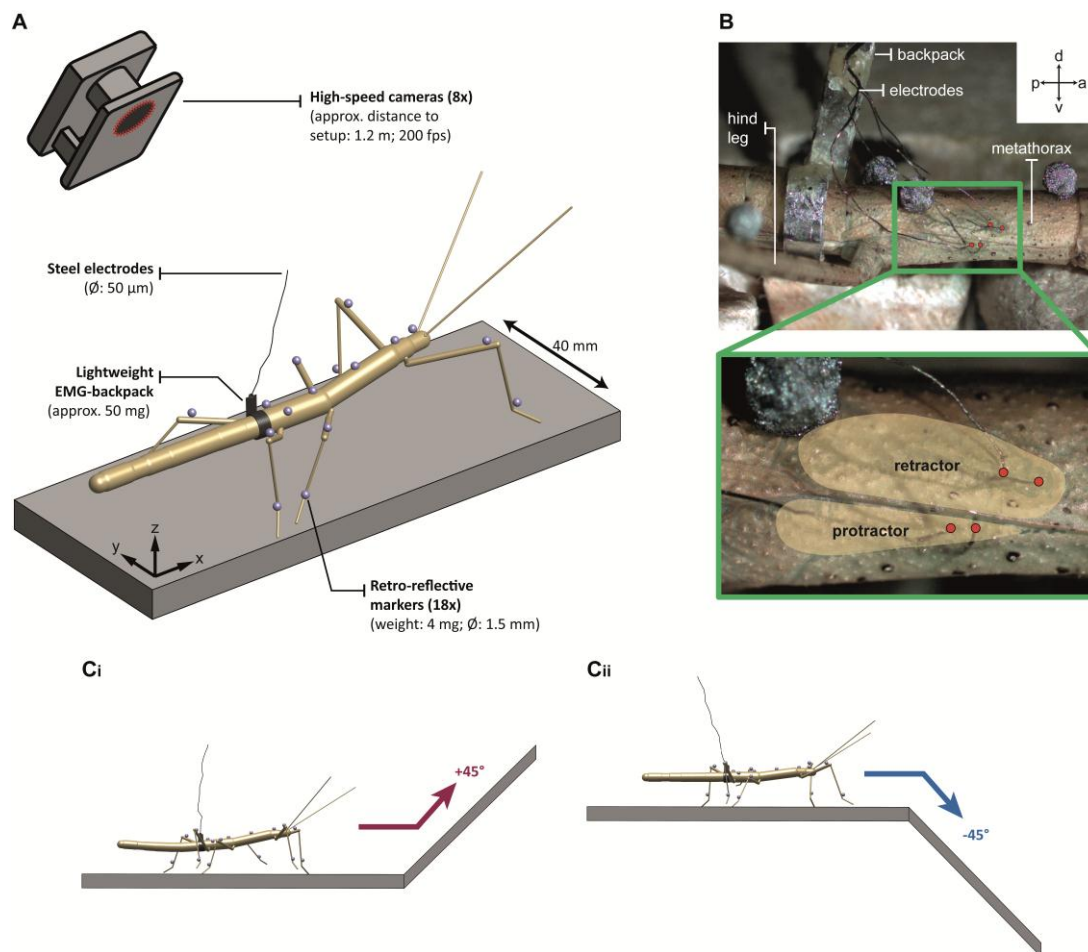
Fig. 1. Combined measurements of whole-body kinematics and muscle activity in unrestrained walking stick insects.

(A) Schematic of a stick insect walking on the horizontal part of the setup. Animals carried 18 retro-reflective motion capture markers (grey spheres) and a light-weight EMG backpack. Eight high-speed cameras captured marker trajectories. **(B)** Side-view images displaying electrode placement for recordings of hind leg muscle activity. EMGs were recorded from the *retractor coxae,* which moves the leg rearward, and the antagonistic *protractor coxae,* which moves the leg forward. Both muscles are located in the metathorax and are attached dorsally (retractor) and dorso-laterally (protractor) to the cuticle. **(C)** Schematic side view of the walkway. Animals were challenged with a step-change in slope from level to either +45° upward walking (C_i) or -45° downward walking (C_{ii}).
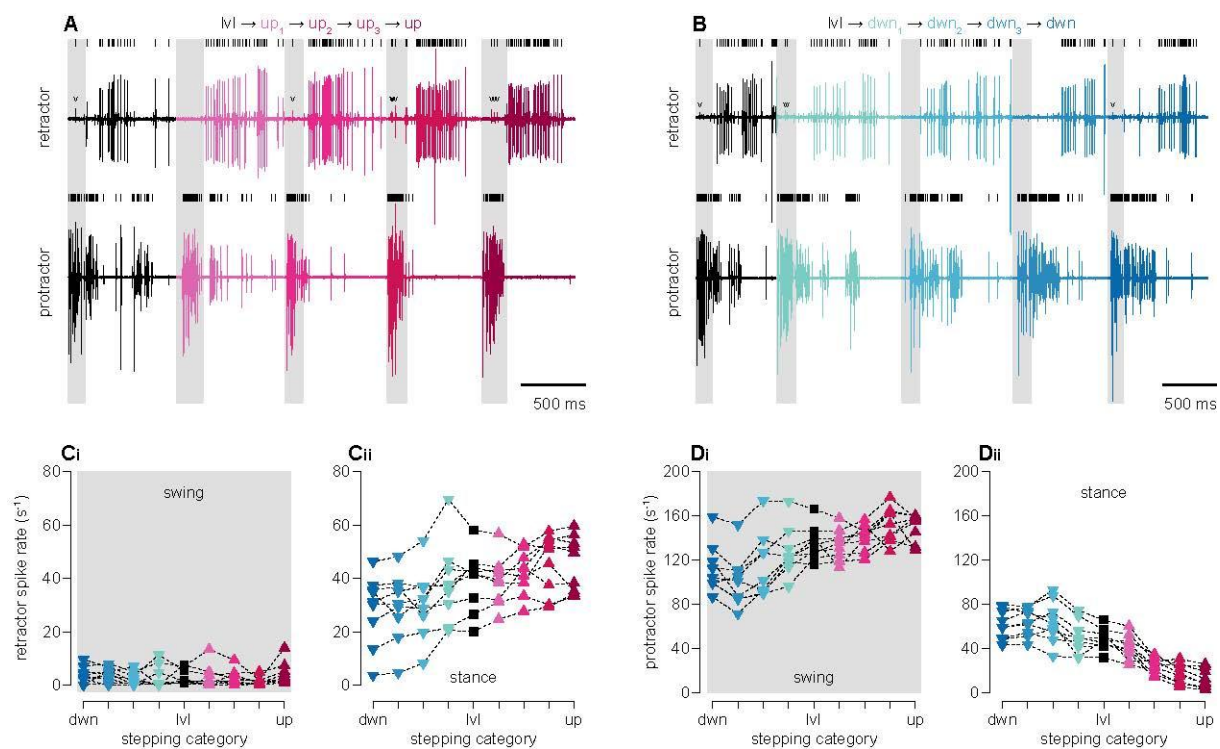
Fig. 2. Activity of antagonistic muscles of a hind leg during the transition from level to slope walking.

(A) Representative raw EMG recordings from antagonistic hind leg muscles during the transition from level to upward walking. Traces are color-coded according to the current step category. Gray areas indicate swing movements. Vertical lines above traces indicate identified spikes based on amplitude. v symbols indicate identified crosstalk. **(B)** Same as A, but for the transition from level to downward walking. **(C)** Mean motoneuron spike rate of the retractor muscle (swing: C_i; stance: C_{ii}) across step categories. Same color code as in A. Note that spike rates were calculated for entire stance phases, despite most of the load-dependent change in activity occurring in the first half of the stance phase. **(D)** Same as C, but for the protractor.
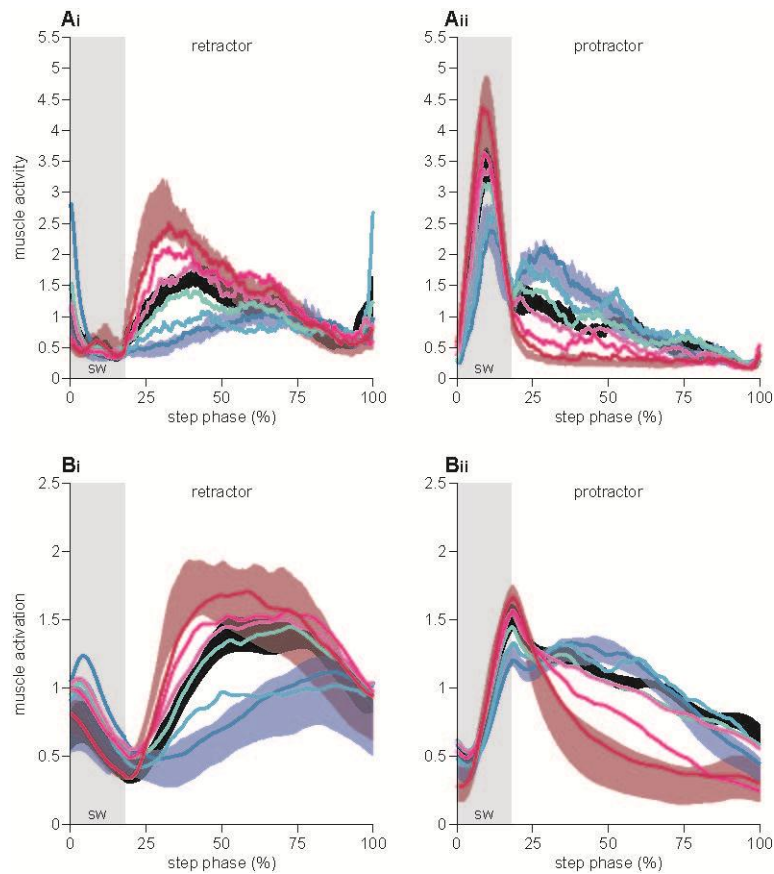
Fig. 3. Hind leg muscle activity and activation during the transition from level to slope walking.

(A) Relative muscle activity for the transition from level to slope walking. Signals were normalized to the step phase. Traces are color-coded according to the current step category, as shown in Fig. 2. . Gray areas indicate swing movements. Error bands show 95 % confidence intervals of per-animal means for steady-state level and slope walking. Transition steps are shown as means of animal means. **(B)** Estimated muscle activation γ according to Harischandra *et al.* (2019). Same plot details as in A.
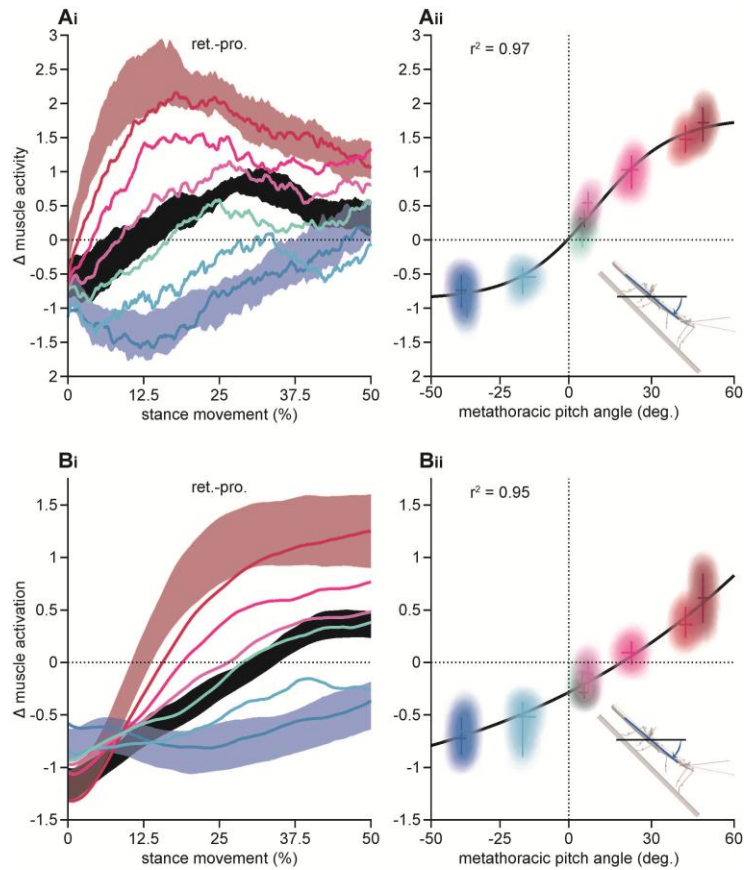
Fig. 4. Co-contraction of retractor and protractor is adjusted during the transition from level to slope walking.

(A) Difference between retractor and protractor muscle activity shown as a time course over the first half of the stance movement (A_i) and the resulting correlation of the average difference during this section with the metathoracic pitch angle (A_{ii}). In A_i, error bands show 95 % confidence intervals of animal means for steady-state level and slope walking. Transition steps are shown as means of animal means. In A_{ii}, distributions are estimated by a bootstrap approach with 5'000 samples around the mean. Superimposed crosses indicate 95 % confidence intervals in both x- and y-direction. The coefficient of determination (r^2) is estimated by fitting a logistic function to the distribution clouds. The schematic insert illustrates the calculation of the pitch angle. **(B)** Same as A, but for muscle activation γ.
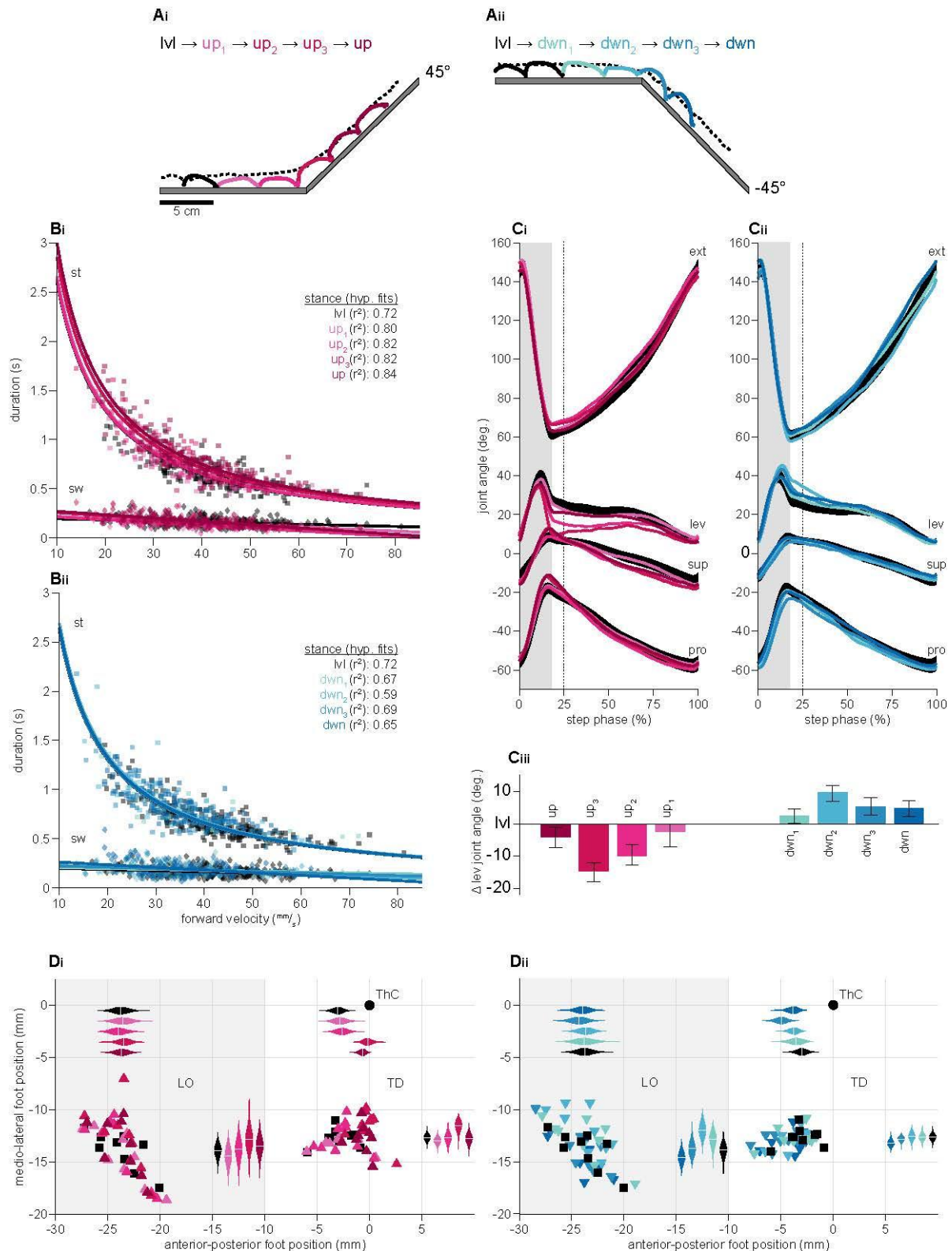
Fig. 5. Hind leg kinematics during the transition from level to slope walking.

(A) Representative foot trajectories (in side view) during the transition from level to upward (A_i) and downward (A_{ii}) walking. Solid lines show the position of the distal tip of the tibia of the right hind leg. Traces are color-coded according to the current step category. Black dotted lines show the position of the CoM. **(B)** Swing (diamonds) and stance (squares) duration of individual steps as a function of

forward velocity during the transition from level to upward (B_i) and downward (B_{ii}) walking. Superimposed are either hyperbolic fits for stance duration over speed (a / speed; a = 27.06 ± 1.37; r^2 = 0.73 ± 0.09; mean ± s.d.) or linear fits for swing duration over speed (a * speed + b; a = -0.002 ± -9.07*10^{-4}; b = 0.25 ± 0.04; r^2 = 0.20 ± 0.17; mean ± s.d.). Coefficients of determination for each hyperbolic fit are stated in the legends. Same color code as in A. **(C)** Hind leg joint angle time courses for the transition from level to upward (C_i) and downward (C_{ii}) walking. Shown are extension (ext), levation (lev), supination (sup), and protraction (pro) angles, normalized to the step phase. Grey areas indicate swing movements. Joint angle time courses for steady-state level walking are depicted as 95 % confidence intervals of animal means, while all other step categories are shown as means of animal means. Same color code as in A. The deviation from level walking in the levation joint angle after 25% of the step is shown for each step category in C_{iii}. Here error bars indicate 95 % confidence intervals. **(D)** Lift-off (LO) and touch-down (TD) positions during the transition from level to upward (D_i) and downward (D_{ii}) walking. Values are in body-centered coordinates with (0,0) marking the ThC joint. Individual points are animal means. Violin plots indicate distributions (5'000 bootstrap samples around the mean) of the animal means in medio-lateral and anterior-posterior foot position for both LO and TD. Gray areas indicate the LO region.
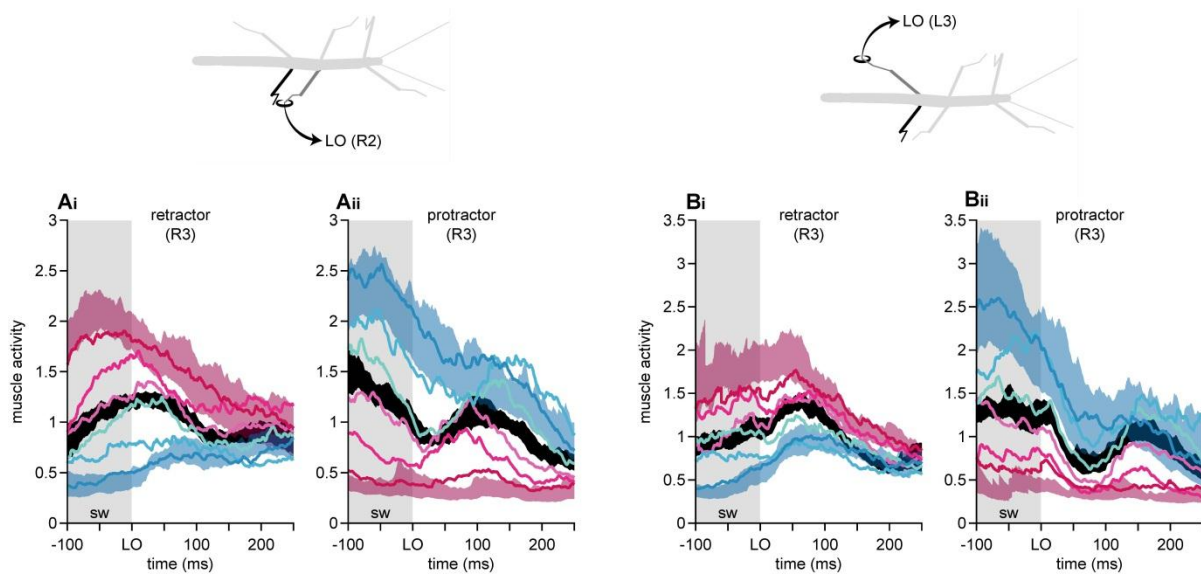
Fig. 6. Lift-off events of neighboring legs trigger transient changes in hind leg muscle activity.

Retractor and protractor muscle activity of the right hind leg was aligned with respect to a lift-off (LO) event of a neighboring leg. Schematics display the two types of lift-off events and typical postures of neighboring legs. **(A)** Response to lift-off of the ipsilateral right middle leg (R2). Time courses show relative retractor (A_i) and protractor (A_{ii}) muscle activity of the right hind leg (R3). Traces are color-coded according to the current step category, as shown in Fig. 2. Error bands show 95 % confidence intervals of animal means for steady-state level and slope walking. Transition steps are shown as means of animal means. Gray areas indicate swing movements of R2. **(B)** Response to lift-off of the contralateral hind leg (L3). Same graph details as in A.
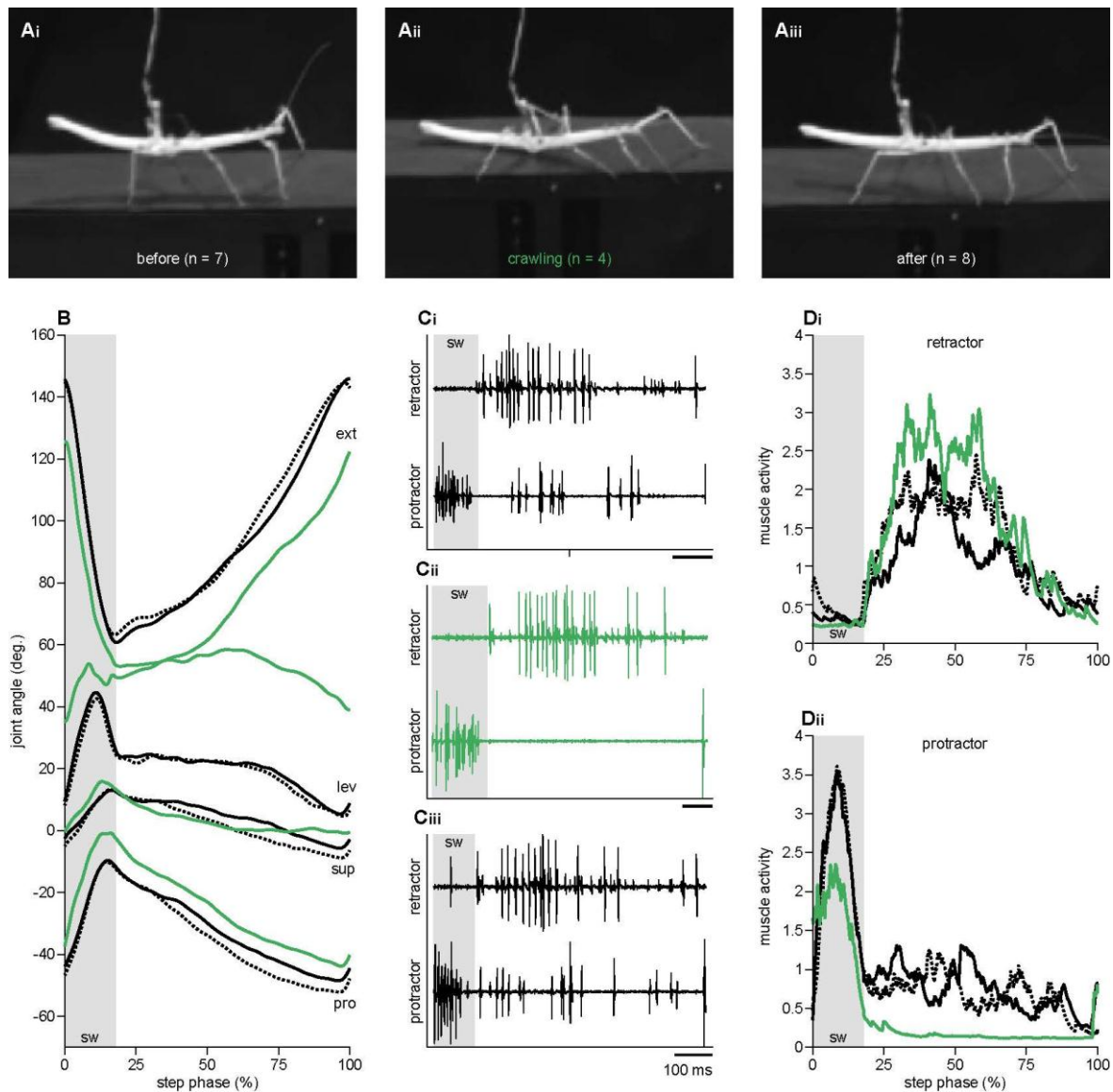
Fig. 7. Hind leg muscle activity depends on whether or not legs support body weight.

(A) Side-view images showing the posture of an animal during regular walking, *i.e.* without ground contact of the body before (A$_i$) and after (A$_{iii}$) a crawling episode, *i.e.*, with the body sliding along the ground (A$_{ii}$). Data are from a single recording session of one animal. **(B)** Hind leg joint angle time courses for steps of regular walking before sliding behavior occurred (black dotted line), during steps with thoracic ground contact, *i.e.* sliding (solid green line), and for steps with rescued posture (solid black line). Shown are extension (ext), levation (lev), supination (sup), and protraction (pro) angles, normalized to the step phase with the grey area indicating the swing movement. **(C)** Exemplary raw EMG recordings of individual steps before (C$_i$), during (C$_{ii}$), and after (C$_{iii}$) sliding behavior. Gray areas indicate swing movements. **(D)** Relative muscle activity for the three posture instances. Signals were normalized to the step phase. Traces are color-coded in the same way as joint angle time courses in A. Gray areas indicate swing movements.

Table 1. Number of performed steps for each step category.

Step category	Valid trials
dwn	154 [5, 28; N=9]
dwn_3	76 [4, 17; N=9]
dwn_2	54 [2, 11; N=9]
dwn_1	59 [3, 11; N=9]
lvl	273 [11, 53; N=9]
up_1	65 [2, 12; N=9]
up_2	60 [3, 13; N=9]
up_3	77 [3, 14; N=9]
up	172 [8, 26; N=9]
Σ	990

The number of successfully executed step cycles of the right hind leg in each of the nine step categories. Values in brackets give the minimum and the maximum number of steps over all animals. lvl, steady-state level walking; up, steady-state upward walking; up_{1-3}, transition steps 1-3 to upward walking; dwn, steady-state downward walking; dwn_{1-3}, transition steps 1-3 to downward walking.
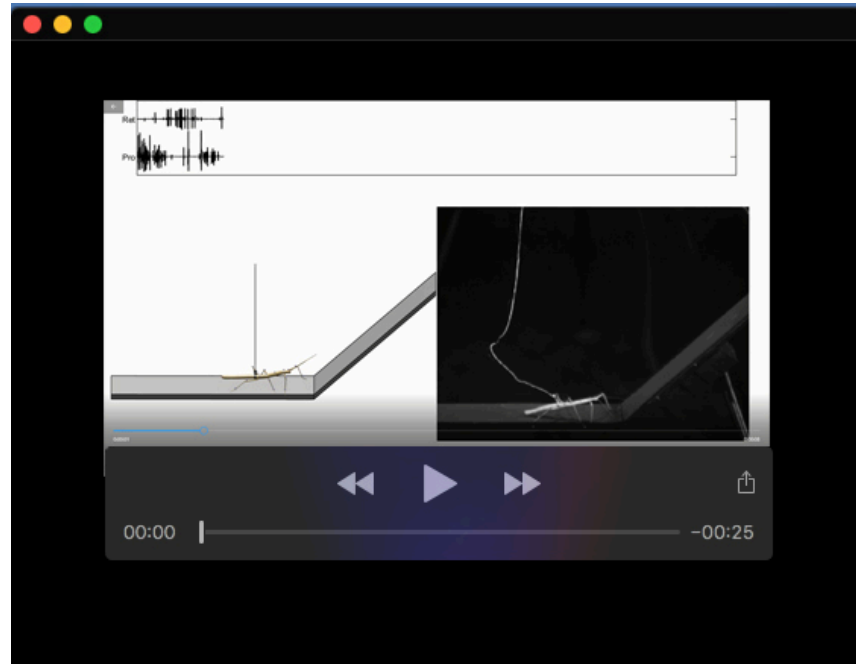
Movie 1. Illustration of the combined measurements of whole-body kinematics and muscle activity for the transition to upward walking. **(Top row)** Raw EMG recordings from antagonistic hind leg muscles retractor (Ret) and protractor (Pro). **(Left panel)** 3D motion-capture-based schematic animation of a stick insect walking freely along a walkway with a step-change in slope from level to +45° upward walking. **(Right panel)** Complementary, synchronized side-view video used for visual validation and movement annotation.
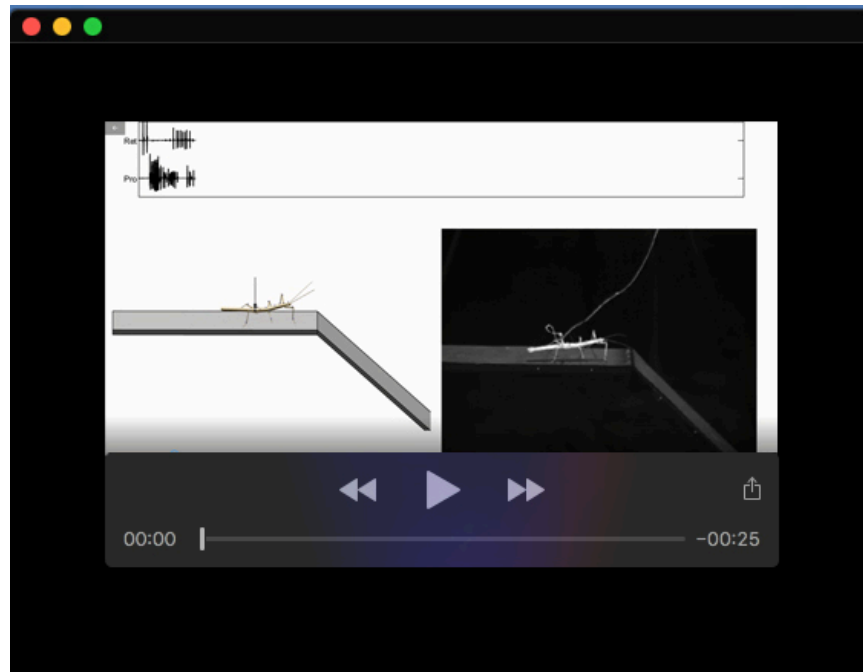
Movie 2. Illustration of the combined measurements of whole-body kinematics and muscle activity for the transition to downward walking. **(Top row)** Raw EMG recordings from antagonistic hind leg muscles retractor (Ret) and protractor (Pro). **(Left panel)** 3D motion-capture-based schematic animation of a stick insect walking freely along a walkway with a step-change in slope from level to -45° downward walking. **(Right panel)** Complementary, synchronized side-view video used for visual validation and movement annotation.